Diffusion, De-excitation, and Three-Body Collision Coefficients for Excited Neon Atoms

A. V. PHELPS
Westinghouse Research Laboratories, Pittsburgh, Pennsylvania
(Received December 31, 1958)

Diffusion coefficients, de-excitation cross sections, and three-body collision coefficients for neon atoms of the $1s^22s^22p^53s$ configuration are obtained from optical absorption measurements of relative decay rates and relative densities of excited atoms following a pulsed discharge. Atoms in the lower metastable ($^3P_2$) and the lower radiating ($^3P_1$) states are destroyed by diffusion to the wall, three-body collisions involving two ground state atoms, and the escape of imprisoned resonance radiation. The diffusion coefficient at unit neon density and 300°K for the metastable states is 5.5×10^{18} cm^{-1} sec^{-1}. The rate of escape of resonance radiation agrees with the predictions of Holstein's theory. At 300°K the average cross section for collisional de-excitation of $^3P_1$ atoms to the $^3P_2$ state is 5×10^{-19} cm^2 and is about 6×10^{-20} cm^2 for the $^3P_0$ to $^3P_1$ and $^3P_0$ to $^3P_2$ transitions. The cross section for the $^3P_1$ to $^3P_2$ de-excitation increases by an order of magnitude between 200°K and 500°K and is three times larger for de-excitation by helium than by neon at 300°K. The three-body collision coefficient for the $^3P_2$ state is 5×10^{-34} cm^6/sec at 300°K and 5×10^{-35} cm^6/sec at 77°K. Estimates of average cross sections for de-excitation by thermal electrons give 10^{-13} cm^2 for the $^3P_1$ to $^3P_2$ process and 10^{-14} cm^2 for the $^3P_0$ to $^3P_1$ transition.

I. INTRODUCTION

SINCE the original measurements of the lifetimes of the metastable states of neon by Meissner and Dorgelo,[1] a number of attempts have been made to account for the observed pressure dependence of the lifetime in terms of the processes responsible for the destruction of the metastables.[2–4] More recently, it became apparent that the metastable destruction could not be accounted for simply by assuming that the metastable atoms are destroyed upon diffusion to the wall and by excitation to a radiating state.[5,6] Furthermore, it was found that except for the lower metastable state, the rates of decay of the excited atom density varied strongly with the intensity of the discharge used to create the metastables.[6] This difficulty has been overcome by Dixon and Grant.[7]

In this paper, it will be shown that the observed dependence of the lifetime of the lower metastable state of neon on gas density and the size of the absorption cell can be explained by assuming that the metastables are destroyed upon diffusion to the wall of the absorption cell, by excitation to the nearest radiating state in a collision with a neutral atom, and by three-body collisions involving two neutral atoms. It is necessary to take into account the imprisonment of the resonance radiation emitted by the radiating state.[2,8] The destruction of the upper metastable state is quantitatively accounted for when experimental conditions are such that the destruction by slow electrons is negligible. Finally, estimates are made of the coefficients for the interactions of electrons with the metastable atoms.

II. THEORETICAL EXPRESSIONS FOR DECAY FREQUENCIES

Figure 1 shows a simplified term level diagram for neon with the ground state, the four states of the $1s^22s^22p^53s$ configuration and one of the ten states of the $1s^22s^22p^53p$ configuration.[9] The $^3P_2$ and $^3P_0$ states are metastable because of selection rules forbidding electric dipole radiation to the ground state. The $^1P_1$

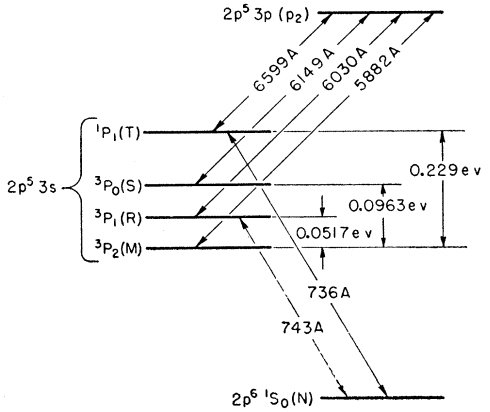

FIG. 1. Simplified energy level diagram for neon showing the ground states, the four levels of the $1s^22s^22p^53s$ configuration, and one level of the $1s^22s^22p^53p$ configuration. In the $2p^53s$ configuration the $^3P_2$ and $^3P_0$ states cannot radiate electric dipole radiation in transitions to the ground state and so are metastable. The $^3P_1$ and $^1P_1$ states emit the 743A and 736A lines, respectively.

[1] K. W. Meissner, Ann. Physik **76**, 124 (1925); and H. B. Dorgelo, Z. Physik **34**, 766 (1925).
[2] W. de Groot and F. M. Penning, *Handbuch der Physik* (Verlag Julius Springer, Berlin, 1933), Chap. 2, Sec. 82.
[3] A. G. C. Mitchell and M. W. Zemansky, *Resonance Radiation and Excited Atoms* (The Macmillan Company, New York, 1934) Chap. IV, Sec. 13.
[4] J. M. Anderson, Can. J. Research **2**, 13 (1930); and **7**, 434 (1932).
[5] F. A. Grant, Phys. Rev. **84**, 844 (1951); F. A. Grant and A. D. Krumbein, Phys. Rev. **90**, 59 (1953); and D. J. Eckl, Can. J. Phys. **31**, 804 (1953).
[6] A. V. Phelps and J. P. Molnar, Phys. Rev. **89**, 1202 (1953).
[7] J. R. Dixon and F. A. Grant, Phys. Rev. **107**, 118 (1957).
[8] A. V. Phelps, Phys. Rev. **99**, 1657(A) (1955); and **100**, 1230(A) (1955).
[9] The energy levels are taken from C. E. Moore, *Atomic Energy Levels*, National Bureau of Standards Circular No. 467 (U. S. Government Printing Office, Washington, D. C., 1949), Vol. I, p. 77. The Paschen notation listed in this reference is used for the states of the $1s^22s^22p^53p$ configuration.

state radiates to the ground state by an allowed electric dipole transition. The $^3P_1$ state can radiate to the ground state as a result of mixing of the singlet and triplet wave functions, i.e., lack of pure Russel-Saunders coupling.[10] We are interested in determining those processes which return the excited atoms to the ground state. Figure 1 shows that the $^3P_1$, $^3P_0$, and $^1P_1$ states lie 0.0517, 0.0963, and 0.229 electron volts above the $^3P_2$ state[9] so that at 300°K ($kT/e=0.026$ ev) an appreciable fraction of the neutral atoms will be capable of causing transitions between the excited states. This means that any analysis of the loss of metastables must allow for the conversion of atoms in the metastable states into atoms in the radiating states. Furthermore, the fact that the radiating states of the $2p^53s$ configuration are resonance states means that the radiation will be rapidly absorbed by atoms in the ground state and the effective lifetime of the radiating state will be several orders of magnitude larger than the natural lifetime.[11,12] As a result of this imprisonment of the resonance radiation, one must also consider the possibility of collisional de-excitation of an atom in a radiating state to the metastable state.

Our experimental studies of helium metastable atoms lead us to expect that the neon metastable atoms will be destroyed upon diffusion to wall of the absorption cell and by three-body collisions between the excited atom and two normal atoms.[13] We make the assumption that, unless otherwise stated, the densities of electrons and metastables are low enough so that collisions between electrons and excited atoms and between two excited atoms can be neglected. Because of the small diffusion coefficients expected for atoms in excited states which can radiate to the ground state, the loss of radiating atoms by ordinary diffusion can be neglected in the range of absorption cell sizes and normal atom densities considered in this paper.[14] We assume that because of the large conversion of potential energy into kinetic energy required, collisional de-excitation of the metastables and resonance atoms to the ground state can be neglected. We also assume that collision-induced radiation[13] is negligible.

These considerations can be formulated mathematically by writing the integro-differential equations which we expect to govern the time dependence of the concentrations of atoms in the various states. In these equations we will designate the densities of atoms in the $2p^6(^1S_0)$ ground state by N, the $2p^53s(^3P_2)$ atoms by M, $2p^53s(^3P_1)$ atoms by R, $2p^53s(^3P_0)$ by S, and the $2p^53s(^1P_1)$ atoms by T. Assuming that M, R, S, and T are small compared to N

$$\frac{\partial M(r,t)}{\partial t}=\frac{-D_M}{N}\nabla^2M-\gamma_MN^2M-(aA+bB+cC)NM+ANR+BNS+CNT, \quad (1)$$

$$\frac{\partial R(\mathbf{r},t)}{\partial t}=-\frac{R}{\tau_R}+\frac{1}{\tau_R}\int R(\mathbf{r}',t)G(|\mathbf{r}'-\mathbf{r}|)\mathbf{dr}'-(A+eE+fF)NR+aANM+ENS+FNT, \quad (2)$$

$$\frac{\partial S(r,t)}{\partial t}=\frac{D_S}{N}\nabla^2S-\gamma_SN^2M-(B+E+gG)NS+bBNM+eENR+GNT, \quad (3)$$

$$\frac{\partial T(\mathbf{r},t)}{\partial t}=-\frac{T}{\tau_T}+\frac{1}{\tau_T}\int T(\mathbf{r}',t)G(|\mathbf{r}'-\mathbf{r}|)\mathbf{dr}'-(C+F+G)NT+cCNM+fFNR+gGNS, \quad (4)$$

where D_U is the diffusion coefficient at unit normal atom density for species U; γ_U is the three-body collision coefficient at unit density; A, B, C, E, F, and G are the frequencies at unit atom density at which atoms in the various upper states will be de-excited to a lower state; the coefficients a, b, c, e, f, and g are the ratios of the frequencies of excitation to the frequencies of de-excitation; τ_R and τ_T are the natural lifetimes of the $^3P_1$ and $^1P_1$ states, respectively; and $G(|\mathbf{r}'-\mathbf{r}|)$ is the probability that radiation emitted at $\mathbf{r}'$ will be absorbed at $\mathbf{r}$ as defined by Holstein.[11] The various de-excitation processes, their symbols, and the difference in energy between the initial and final states are listed in Table I.

The de-excitation frequencies at unit density, X, are defined in terms of the de-excitation cross section, $Q(v)$, by the equation

$$X=\int_0^\infty vQ(v)f(v)dv, \quad (5)$$

where v is the relative speed of the colliding particles and $f(v)dv$ is the fraction of the collisions in which the relative speed is between v and $v+dv$. Similarly, the frequency of excitation at unit density is given by

$$X'=\int_{v_0}^\infty vq(v)f(v)dv, \quad (6)$$

TABLE I. De-excitation processes and symbols for de-excitation frequencies at unit density.

Upper state	Lower state	Symbol	Energy difference (e.v.)
$^3P_1(R)$	$^3P_2(M)$	A	0.0517
$^3P_0(S)$	$^3P_2(M)$	B	0.0963
$^1P_1(T)$	$^3P_2(M)$	C	0.229
$^3P_0(S)$	$^3P_1(R)$	E	0.0446
$^1P_1(T)$	$^3P_1(R)$	F	0.177
$^1P_1(T)$	$^3P_0(S)$	G	0.133

[10] G. H. Shortley, Phys. Rev. **47**, 295 (1935).
[11] T. Holstein, Phys. Rev. **72**, 1212 (1947); and **83**, 1159 (1951).
[12] L. M. Biberman, J. Exptl. Theoret. Phys. U.S.S.R. **17**, 416 (1947); and **59**, 659 (1948).
[13] A. V. Phelps, Phys. Rev. **99**, 1307 (1955).
[14] A. V. Phelps and A. O. McCoubrey, Bull. Am. Phys. Soc. Ser. II, **3**, 83 (1958).

TABLE II. Ratio of excitation frequency to de-excitation frequency.

Transition	$^3P_1-{}^3P_2$	$^3P_0-{}^3P_2$	$^1P_1-{}^3P_2$	$^3P_0-{}^3P_1$	$^1P_1-{}^3P_1$	$^1P_1-{}^3P_0$
Symbol	a	b	c	e	f	g
Value at 300°K	8.08×10^{-2}	4.76×10^{-3}	8.40×10^{-5}	5.91×10^{-2}	1.042×10^{-3}	1.755×10^{-2}

where $q(v)$ is the cross section for excitation and v_0 is the speed corresponding to the excitation energy. The ratio of the frequency of excitation to the frequency of de-excitation is obtained from the principle of detailed balancing[15] and is given by

$$X/X'=(2J_1+1)(2J_2+1)^{-1}e^{-\Delta E/kT}, \tag{7}$$

where J_2 and J_1 are the J values for the upper and lower states, ΔE is the energy separation between states, k is the Boltzman constant and T is the absolute temperature of the gas. The ratio given by Eq. (7) is also a measure of the fraction of neon atoms with energy greater than ΔE and, therefore, of the atoms able to cause excitation.

We do not know how to solve the partial integro-differential Eqs. (1) through (4). Therefore, we shall assume that the spatial distributions of the excited atoms are close to those of the fundamental modes for the diffusion and imprisonment problems, i.e., that

$$D\nabla^2U=-DU/\Lambda^2, \tag{8}$$

and

$$\frac{U(\mathbf{r})}{\tau_U}-\frac{1}{\tau_U}\int U(\mathbf{r}')G(|\mathbf{r}'-\mathbf{r}|)\mathbf{dr}'=\nu_{IU}U(\mathbf{r}), \tag{9}$$

where $\Lambda=R/2.405$ for an infinite cylindrical container and ν_{IU} is the decay constant or reciprocal lifetime for the decay of imprisoned resonance radiation as calculated by Holstein.[11] The errors introduced by assumptions of this kind have been studied by Walsh.[16] In our experiments the gas density is sufficiently high so that we expect that the escape of the resonance radiation is controlled by the pressure broadening of the resonance line. In this case, Walsh shows that Eq. (9) gives a rate of escape which is: (a) 3% too small when the density of excited atoms is zero at the wall, as when diffusion dominates the decay; (b) correct when the escape of the resonance radiation is the dominant loss process; and (c) about 20% too small when the density of excited atoms is independent of position. Since Eqs. (1) through (4) do not contain any terms tending to make the excited atom density independent of position, as do the electron excitation and de-excitation terms considered by Walsh, the error introduced by Eq. (9) is expected to be less than about 10% or of the order of the accuracy claimed for the calculation of ν_{IU}.

The imprisonment decay constant, ν_{IU}, can be calculated from Holstein's theory[11] and the natural lifetime of the radiating state using the relation

$$\nu_{IU}=0.205(1/\tau_U)(\lambda/R_0)^{\frac{1}{2}}, \tag{10}$$

where λ is the wavelength of the resonance radiation and R_0 is the radius of the absorption cell. This relationship assumes (a) that the neon density is high enough so that the escape of the resonance radiation is determined by the pressure broadened portion of the resonance line rather than the Doppler broadened portion of the line, (b) that the dominant interaction between an excited neon atom and a normal neon atom is of the dipole-dipole type studied by Furssov and Vlassov,[17] and (c) that the effect of hyperfine structure due to isotope shift can be neglected. Calculations of the effects of Doppler broadening and hyperfine structure[18] show that Eq. (10) should be satisfactory for neon densities above about 3×10^{17} atom/cc. The major uncertainties are the values for the natural lifetimes for the $^1P_1$ and $^3P_1$ states. The natural lifetime of the $^1P_1$ state has been measured by Schütz and Schillbach[19] to be $(1.2\pm0.6)\times10^{-9}$ sec. The ratio of the natural lifetime of the $^3P_1$ state to that for the $^1P_1$ state has been calculated by Shortley[10] to be 13.2 ± 0.1. Therefore, the natural lifetime of the $^3P_1$ state should be $(1.6\pm0.8)\times10^{-8}$ seconds. These values can be substituted into Eq. (10) to give predicted values for the decay constants for the resonance radiation. The only coefficients in Eq. (1)–(4) which we know *a priori* are the ratios of the frequencies of excitation and de-excitation. These are listed in Table II for neon atoms at 300°K. The neglect of departures from lowest decay mode spatial distributions as indicated by Eqs. (8) and (9), reduce Eqs. (1)–(4) to a set of first order linear equations with twelve interaction coefficients.

[15] See reference 3, p. 57.

[16] P. J. Walsh, Phys. Rev. **107**, 338 (1957).

[17] V. Furssov and A. Vlassov, Physik. Z. Sowjetunion **10**, 378 (1936). See reference 11 for the application of this work to the imprisonment problem.

[18] L. M. Biberman and I. M. Gurevich, J. Explt. Theoret. Phys. U.S.S.R. **20**, 108 (1950); and P. J. Walsh (private communication). The theory developed by Biberman and Gurevich assumes that impact broadening and natural broadening produce the same effects on imprisonment. However, Holstein (reference 11) points out that when natural broadening dominates, the assumption of identical and uncorrelated absorption and emission spectra used in imprisonment theory is not valid. As a first approximation we have included natural broadening in the absorption spectrum but not in the emission spectrum. If we also include the effects of isotopic hyperfine structure the theory of Walsh can be used to show that at densities of about 10^{17} atom/cc there is a reduction in ν_{IR} of as much as 50% below the limiting value given by Eq. (1).

[19] W. Schütz, Ann. Physik **18**, 705 (1933); and H. Schillbach, Ann. Physik **18**, 721 (1933). Very recent theoretical calculations give life times about twice as large as these experimental values. See A. Gold and R. S. Knox, Phys. Rev. **113**, 834 (1959).

The differential equations can now be written as

$$\nu_M=-\frac{1}{M}\frac{dM}{dt}=\frac{D_M}{N\Lambda^2}+\gamma_M N^2+aAN\left(1-\frac{R}{aM}\right)+bBN\left(1-\frac{S}{bM}\right)+cCN\left(1-\frac{T}{cM}\right), \quad (11)$$

$$\nu_R=-\frac{1}{R}\frac{dR}{dt}=\nu_{IR}+AN\left(1-\frac{aM}{R}\right)+eEN\left(1-\frac{S}{eR}\right)+fFN\left(1-\frac{T}{fR}\right), \quad (12)$$

$$\nu_S=-\frac{1}{S}\frac{dS}{dt}=\frac{D_S}{N\Lambda^2}+\gamma_S N^2+BN\left(1-\frac{bM}{S}\right)+EN\left(1-\frac{eR}{S}\right)+gGN\left(1-\frac{T}{gS}\right). \quad (13)$$

Here ν_M, ν_R, and ν_S are the instantaneous decay frequencies, or slopes of semilogarithmic plots of density as a function of time, for the $^3P_2$, $^3P_1$, and $^3P_0$ states. In general, the values of the decay frequencies are functions of time. The terms of the form of $aAN\times(1-R/aM)$ are the net frequencies of destruction of the state for which the equation is written. In this case, aAN is the frequency of $^3P_2$ destruction by excitation and ANR/M is the frequency of $^3P_2$ production by de-excitation of $^3P_1$ atoms. We have omitted the equation for the $^1P_1$ state since the experiments to be discussed below give no information regarding the $^1P_1$ decay frequency. Because of coupling between these equations the decay frequencies for the various levels will become equal and constant at sufficiently late times in the afterglow. In order to use these equations to determine any of the unknown coefficients, except possibly the diffusion coefficients, we must know the relative concentrations of excited atoms in the four states.

III. THEORY OF RELATIVE EXCITED ATOM DENSITY MEASUREMENTS

In this experiment the relative densities of the excited atoms are calculated from measurements of the relative absorption of characteristic radiation by the excited atoms. According to Fig. 1 one could measure the relative absorption produced by the levels of the the $2p^53s$ configuration using the 5882 A, 6030 A, 6146 A, and 6599 A lines. These lines have a common upper state which is designated as the p_2 level of the $2p^53p$ configuration.[9] Since the $2p^53p$ configuration has ten levels there are many lines which can be used for absorption measurements. The lines actually used in the experiments reported below were 5882 A ($p_2-{}^3P_2$), 6096 A ($p_4-{}^3P_1$), 6266 A ($p_5-{}^3P_0$), and 5852 A ($p_1-{}^1P_1$). The 5882 A line was chosen because of its low absorption coefficient and large photomultiplier response while the others were selected to obtain the best compromise between a large absorption coefficient, a large photomultiplier response, and relative freedom from interfering neighboring lines.

The relation between the density of absorbing atoms and the observed absorption has been the subject of a number of investigations.[3,6,7]. When the spectral distribution of the line emitted by the source and the absorption line are determined by Doppler broadening and when the absorption is small

$$n=\frac{(1+\delta^2)^{\frac{1}{2}}}{\sigma_0 L}A_\delta. \quad (14)$$

Here n is the density of absorbing atoms, δ is the ratio of the half-width of the emission line to the half-width of the absorption line, σ_0 is the absorption cross section of the center of the line, L is the absorption path, and A_δ is the measured fractional absorption. Since we shall use only relative densities of atoms in the various excited states we need to know the relative absorption coefficients for the lines used. Ladenberg[20] and Shortley[10] have obtained sets of relative f values and line strengths from measurements of relative dispersion and relative intensity of emission of the lines in the $2p^53s$ to $2p^53p$ transitions. Instead of using this data to calculate relative absorption coefficients, we have used the more recent data of Krebs[21] and of Garbuny[22] to calculate a new set of relative line strengths. The analysis of the experimental data using Shortley's theory[10] is given in the Appendix and the relative absorption coefficients of interest to us are given in Table III. Phelps and Molnar[6] obtained a value of $\delta=1.5$ for the type of source used in the experiments described below. Dixon and Grant[7] obtained essentially the same value for a similar source for the lines we shall use in the analysis of their data. Since δ is essentially the same for all lines used we do not need to know it accurately unless we wish to determine densities of excited atoms

TABLE III. Relative absorption cross sections for lines used in experiments.

Transition	Wavelength (A)	Relative absorption coefficient
$^3P_2-p_2$	5882	1
$^3P_2-p_4$	5945	1.7
$^3P_1-p_4$	6096	5.3
$^3P_1-p_2$	6074	3.8
$^3P_0-p_5$	6266	14.1
$^1P_1-p_1$	5852	5.0

[20] R. Ladenburg, Revs. Modern Phys. **5**, 243 (1933); and R. Ladenburg and S. Levy, Z. Physik **88**, 461 (1934).

[21] K. Krebs, Z. Physik **101**, 604 (1936). The author wishes to thank Dr. M. Garbuny for bringing references 21 and 22 to his attention.

[22] M. Garbuny, Z. Physik **107**, 362 (1937).

at large values[23] of A_δ. The effect of pressure broadening on the relative absorptions has not been investigated experimentally but is believed to be small for all states except the $^1P_1$ state since the broadening is small and all lines are broadened by about the same amount.[24] Since we do not observe absorption by atoms in the $^1P_1$ state, we neglect pressure broadening effects.

IV. EXPERIMENT

The experimental apparatus used in these studies of neon is the same as that used to study the metastable states of helium.[13] The reader is referred to the previous work for a detailed description of the same sampling technique.[25] The neon excited atoms are produced by applying a short ($\sim$20 μsec) high voltage ($\sim$15 kv and $\sim$2 ma) pulse between electrodes at the end of a long cylindrical absorption cell. The light from a 0.5 diameter capillary discharge tube was collimated and passed along the axis of the absorption cell to a Hilger visible monochromator ($\sim f/12$). The monochromator was adjusted for about 8 A resolution at 6400 A. The light from the line whose absorption was being measured was allowed to fall on the cathode of an RCA 1P22 photomultiplier. The absorption signal was measured using time sampling techniques and separated from the signal due to the unabsorbed light using the narrow band amplifier and synchronous detector described previously.[25]

The vacuum system used in these experiments was the same as that used previously.[13] Following an 8-hour bakeout, the ultimate pressure was 10^{-9} mm Hg or less and the rate of rise of pressure was 10^{-9} mm Hg/min or less with no ion pumping by the ionization gauge. The neon samples were "reagent grade" and, as obtained from the Air Reduction Sales Company, were analyzed as being free of impurities to the limit of sensitivity of their tests. In later series of runs, a cataphoresis discharge[26] was operated during the experiments when the pressure was between about 10 and 100 mm Hg. Observation of the cataphoresis spectrum with a low resolution spectrometer showed only neon lines. Except where otherwise noted these experiments were conducted at a room temperature of 300$\pm$5°K. As in the case of helium,[13] the maximum temperature rise of the gas during the short breakdown pulse is calculated to be less than 5°C for a pressure of 1 mm Hg and proportionally less at higher pressures. Experimentally, there was no rise in the wall temperature due to the discharge.

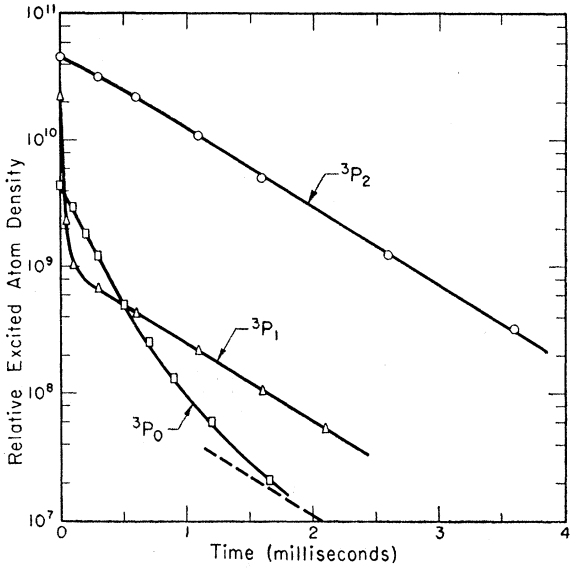

FIG. 2. Relative densities of excited atoms in $^3P_2$, $^3P_1$, and $^3P_0$ states as a function of time following a pulsed discharge with a neon density of 4×10^{17} atom/cc and $\Lambda^2=0.050$ cm^2. The numbers shown on the abscissa are the densities of excited atoms in atoms/cc calculated by assuming that $\sigma_0=7.6\times10^{-13}$ cm^2 for the 5882 A line. This cross section is that obtained by assuming that the f value for the $^3P_2-p_9$ transition is 0.5 as suggested by Ladenberg in reference 20. The dashed line is the asymptotic variation of the $^3P_0$ density as calculated in Sec. VI of the text.

In the later runs an interference filter was placed between the collimated source and the absorption cell so as to illuminate the cell with only lines in the immediate vicinity of the line whose absorption was being measured. This was done in order to reduce the intensity of the unused lines in the monochromator and in the absorption cell. The effect of scattered radiation in the monochromator, principally 6402 A, was to produce a false absorption signal when observing lines such as the 5852 A line. The test for a false absorption was to note whether the apparent fractional absorption was independent of the monochromator setting as the monochromator setting was turned toward the edges of the line. Using this test it was shown that under the conditions of our experiment there was no measurable absorption of the 5852 A line by atoms in the $^1P_1$ state at times later than 100 μsec after the discharge pulse. A second reason for using the interference filters was that it was found that with the source intensities used the radiation was strong enough to reduce the longest observed lifetimes by about 2%.

The lifetime measurements as a function of temperature were made using an absorption cell in an oven whose temperature was controlled using the circuit described by Malmberg and Matland.[27] The temperature was measured using chromel-alumel thermocouples fastened to the cell wall.

[23] Dixon and Grant[7] give curves showing the relation between $N\sigma_0 L$ and A_δ for constant δ and large A. All of the data obtained by the author was taken at low enough densities of excited atoms such that the departures from the curves for a constant value of δ found by Dixon and Grant for $A>0.5$ need not be considered. When the metastable density changes appreciably during the sensitive period of the photomultiplier, the observed absorption signal is an average value and the reconstruction of the actual density variation becomes difficult.

[24] K. Lang, Acta Phys. Austriaca **5**, 376 (1952).

[25] A. V. Phelps and J. L. Pack, Rev. Sci. Instr. **26**, 45 (1955).

[26] A. Riesz and G. H. Dieke, J. Appl. Phys. **25**, 196 (1954).

[27] P. R. Malmberg and C. G. Matland, Rev. Sci. Instr. **27**, 136 (1956).

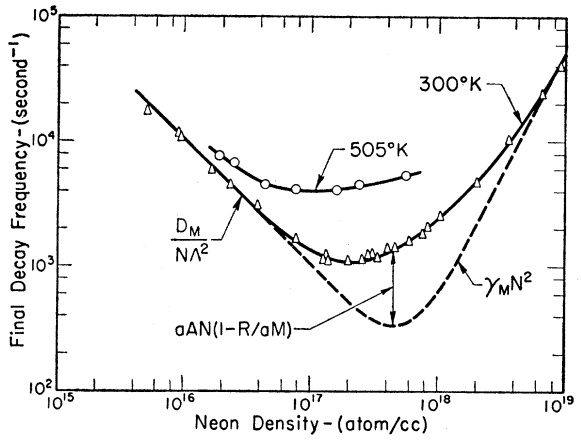

FIG. 3. Final decay frequency for the $^3P_2$ and $^3P_1$ states as a function of neon density at 300°K and 505°K for a discharge tube with $\Lambda^2=0.050$ cm^2. The dashed curve through the 300°K points is the sum of the contributions of metastable loss by diffusion to the wall and by three-body collisions. The solid curves are a fit of Eq. (17) of the text to the experimental points. The difference between the dashed curve and the lower solid curve is the net frequency of excited atom destruction as a result of excitation to the $^3P_1$ radiating state.

V. EXPERIMENTAL RESULTS

An example of the decay curves obtained in this experiment is shown in Fig. 2. Here we have plotted the relative excited atom density as a function of the time by which the photomultiplier pulse is delayed following the discharge pulse. The relative densities were obtained from the measured absorption using Eq. (14) and the relative absorption coefficients given in Table III. These curves show that for times greater than about a millisecond the $^3P_2$ density decays exponentially with time. The $^3P_1$ density decays very rapidly immediately after the discharge and then finally decays with the same decay frequency as does the $^3P_2$ density. The initial decay of the $^3P_0$ density is intermediate, while the decay at later times shows a definite tendency to approach the same decay frequency as that of the $^3P_2$ and $^3P_1$ densities. Note that the initial decay of the $^3P_0$ density is exponential for nearly a factor of ten in density.

Figure 3 shows the measured values for the final decay frequency for the $^3P_2$ and $^3P_1$ states as a function of neon gas density for an absorption cell with a radius of $R=0.54$ cm and a length of $L=30$ cm, i.e., $\Lambda^2=0.050$ cm^2. Qualitatively, this data shows that the final decay frequency is inversely proportional to the gas density at low densities as expected when the dominant loss process is destruction upon diffusion to the wall of the absorption cell. At the highest densities the decay constant appears to approach a square law dependence on gas density as expected when the excited atom destruction is predominantly by three-body collisions. In the intermediate pressure range the dependence of the decay frequency on gas density is complicated by the collisional conversion of excited atoms from one state to another.

Figure 4 shows the ratios of densities of excited atoms when the decay frequencies are equal to the final value. These ratios are obtained from the measured absorption ratios using the relative absorption coefficients given in Table III. At the lower gas densities the densities of the less populated states become too low to allow one to obtain accurate absorption ratios. In some cases, e.g., Fig. 2, we can obtain only an upper limit to the final density ratio and have indicated this by the arrows in Fig. 4.

Information on the decay of the $^3P_0$ density can also be obtained from the decay frequencies measured early in the afterglow provided the electron density is sufficiently low to avoid destruction of the $^3P_0$ metastables in collisions with electrons. The measurements of this decay frequency by Dixon and Grant[7] are considerably more extensive than those of the author and will be used in the analysis of the next section.

VI. ANALYSIS OF DATA

The objective of this section is to show how we have obtained the various interaction coefficients for the excited atoms by fitting the measured decay frequency and relative density data to the theory as expressed by Eqs. (11)–(13). First we shall consider the $^3P_0$ equation, Eq. (13), at early times in the afterglow and at low and intermediate gas densities, since the analysis of the data obtained by Dixon and Grant is especially simple. The results obtained are used to simplify the analyses of the $^3P_2$ and $^3P_1$ equations, Eqs. (11) and (12). The $^3P_1$ equation will be used to find values of the imprisonment decay constant, ν_{IR}, for comparison with the

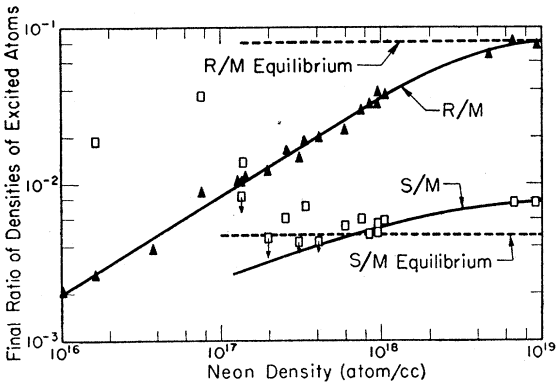

FIG. 4. Ratios of densities of excited neon atoms during final exponential decay as a function of neon density at 300°K and for $\Lambda^2=0.050$ cm^2. The dashed lines give the ratio of densities of excited atoms expected for thermal equilibrium at 300°K, i.e., the R/M and S/M equilibrium ratios are the values of a and b given in Table II. The net frequencies of excitation of $^3P_2$ atoms to the $^3P_1$ and $^3P_0$ states are proportional to the difference between the observed and the equilibrium values of R/M and S/M, respectively. Because of the long times required to reach the final value, the measured values of S/M at low neon densities are probably determined by discharge conditions rather than collisions causing conversion from one state of the $2p^53s$ configuration to another.

predictions of theory as given by Eq. (10). Finally, we shall apply the $^3P_0$ equation to data of Figs. 2, 3, and 4.

$^3P_0$ Analysis at Early Times

Figure 2 shows that at a neon density of 4.0×10^{17} atom/cc the relative density of $^3P_0$ atoms early in the afterglow is considerably larger than at late times and that during this period the initial $^3P_0$ density decay is exponential with a decay frequency significantly larger than the value late in the afterglow. Dixon and Grant have made a detailed study of the decay of the $^3P_0$ density at early times and have found that for sufficiently low discharge currents the decay frequency for the $^3P_0$ atoms is independent of the discharge current and so appears to be free from the effects of destruction by electrons. Under these conditions the data of Fig. 2 and Table II shows that $bM/S\ll1$ and $eR/S\ll1$. Since we expect[28] that $T/gS\ll1$, Eq. (13) can be written as

$$\nu_S=\frac{D_S}{N\Lambda^2}+\gamma_S N^2+(B+E+gG)N. \tag{15}$$

At sufficiently low gas densities the effects of three-body collisions can be neglected relative to diffusion losses and two-body collisions so that Eq. (15) becomes

$$\nu_S N\Lambda^2=D_S+N^2\Lambda^2(B+E+gG). \tag{16}$$

Figure 5 shows a plot of values of $\nu_S N\Lambda^2$ as a function of $N^2\Lambda^2$ using data obtained by Dixon and Grant with $\Lambda^2=2.48$ cm^2 and by the author with $\Lambda^2=0.050$ cm^2 and 2.1 cm^2. From this plot we conclude that at 300°K,

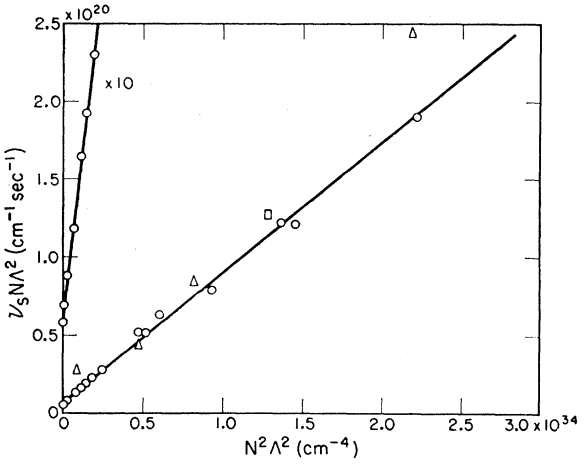

FIG. 5. Determination of diffusion coefficient and sum of two-body collision frequencies for atoms in $^3P_0$ state at 300°K using Eq. (16) of text. The points indicated by circles (○) were obtained by Dixon and Grant with $\Lambda^2=2.48$ cm^2. The data indicated by triangles (△) and the square (□) were obtained by the author with $\Lambda^2=0.050$ cm^2 and 2.1 cm^2, respectively.

[28] The density of $^1P_1$ atoms is expected to be well below the equilibrium values, i.e., $T/gS\ll1$, $T/fR\ll1$, and $T/cM\ll1$. This is due to the fact that the value of ν_{IT} predicted by Eq. (10) is an order of magnitude larger than the maximum de-excitation frequencies found for neon.

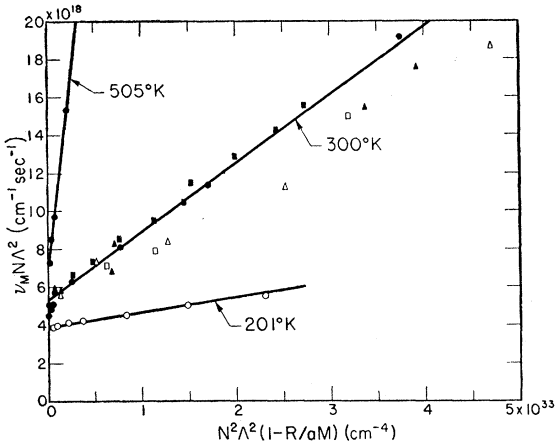

FIG. 6. Determination of diffusion coefficient and excitation frequency for atoms in $^3P_2$ state at various neon temperatures using Eq. (18) of text. The data obtained by various workers are indicated by: (△) with $\Lambda^2=6.67$ cm^2 and (□) with $\Lambda^2=1.89$ cm^2 by Phelps and Molnar; (▲) with $\Lambda^2=3.77$ cm^2 and (●) with $\Lambda^2=0.050$ cm^2 by the author; (■) with $\Lambda^2=2.48$ cm^2 by Dixon and Grant; and (○) with $\Lambda^2=1.00$ cm^2 by Grant and Krumbein.

$D_S=5.8\times10^{18}$ cm^{-1} sec^{-1} and $B+E+gG=8\times10^{-15}$ cm^3 sec^{-1}. This analysis does not allow us to evaluate the individual two-body collision coefficients but does show that $B\leq8\times10^{-15}$ cm^3/sec and $E\leq8\times10^{-15}$ cm^3/sec at 300°K. Now, the theory of excitation transfer[29] shows that in general the cross section for transfer or de-excitation decreases as the potential energy difference between the initial and final states increases. We therefore assume that the value of G will be less than that of B or E because of the larger energy difference between the $^3P_0$ and the $^1P_1$ states (see Table I) than between the $^3P_0$ state and either the $^3P_2$ state of the $^3P_1$ state. If $G<(B+E)$, then $gG<1.5\times10^{-16}$ cm^3/sec and $B+E=8\times10^{-15}$ cm^3/sec.

$^3P_2$ Analysis

Now that we have an upper limit to the two-body coefficient B, we can proceed with the analysis of the $^3P_2$ equation, Eq. (11). This limit combined with the data of Figs. 3 and 4 shows that the maximum value of the term $bBN(1-S/bM)$ at late times is small compared to ν_M and can be neglected in Eq. (11). We assume that the frequency of transitions from the $^1P_1$ state to the $^3P_2$ state is smaller than the frequency of $^3P_1$ to $^3P_2$ transitions, i.e., $C<A$, since Table I shows that the potential energy difference between the initial and final states is much greater in the former case.[29] If $C<A$, then $cC<cA=afA=1.04\times10^{-3}aA$ and we can neglect the $cCN(1-T/cM)$ term[28] in Eq. (11). We are now in a position to evaluate the coefficients D_M, γ_M, and A of the simplified $^3P_2$ equation,

$$\nu_M=D_M/N\Lambda^2+\gamma_M N^2+aAN(1-R/aM). \tag{17}$$

[29] H. S. W. Massey and E. H. S. Burhop, *Electronic and Ionic Impact Phenomena* (Oxford University Press, London, 1952), Chap. VII, Sec. 10.

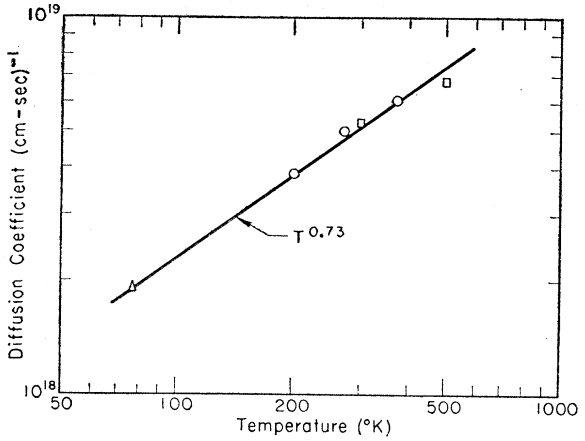

FIG. 7. Diffusion coefficients at unit gas density for neon atoms in the $^3P_2$ state as a function of neon temperature. The symbols used and sources of data are: (□) from the present work, (○) by Grant and Krumbein, and (△) by Phelps and Molnar.

At low neon gas densities the three-body collision term is small compared to the diffusion and excitation terms so that Eq. (17) can be simplified to

$$\nu_M N\Lambda^2 = D_M + aAN^2\Lambda^2(1-R/aM). \quad (18)$$

This equation shows that if we plot the measured values of $\nu_M N\Lambda^2$ as a function of the measured $N^2\Lambda^2 \times(1-R/aM)$ values, the intercept is D_M and slope is aA. Even though we do not know the values of R/M for the earlier experiments we should obtain the same value of aA by plotting $\nu_M N\Lambda^2$ *vs* $N^2\Lambda^2$ provided we limit ourselves to sufficiently low neon densities. Thus, Fig. 6 shows all of the available data in the range of variables covered[30] except at 505°K, where only the low density points fit on this graph. The R/aM correction could be made only in the case of the $\Lambda^2=0.050$ cm^2 data at 300°K and 505°K. The scatter in the 300°K data is large but one must keep in mind that because of the large range of Λ^2 values the data covers a 100 to 1 range of decay frequencies. The resulting diffusion and de-excitation coefficients are plotted as a function of gas temperature in Figs. 7 and 8. The data of Phelps and Molnar[6] and of Grant and Krumbein[5] allows us to set the upper limit to A at 77°K shown in Fig. 8. We shall reserve further comment on these data for Sec. IX.

At the high gas densities the contribution of the diffusion term to Eq. (17) becomes small and it is convenient to rearrange terms as follows:

$$(\nu_M/N^2 - D_M/N^3\Lambda^2) = aA(1-R/aM)/N + \gamma_M. \quad (19)$$

Here we regard D_M as a known quantity determined using Eq. (18). Equation (19) shows that if the values of $(\nu_M/N^2-D_M/N^3\Lambda^2)$ are plotted as a function of the measured values of $(1-R/aM)/N$, the slope is the excitation coefficient aA and the intercept is the three-body coefficient, γ_M. This is done in Fig. 9 for the data shown in Figs. 3 and 4 and yields the values of $A=4.1\times10^{-14}$ cm^3/sec and $\gamma_M=5.0\times10^{-34}$ cm^6/sec. Figure 9 makes use also of data obtained by Dixon[31] using the 5945 A ($^3P_2-p_4$) and 6074 A ($^3P_1-p_3$) lines to measure the relative densities in an absorption cell with $\Lambda^2=2.48$ cm^2.

The solid curve of Fig. 3 is a fit of Eq. (17) over the complete range of neon density. It represents a compromise between the results obtained with Eqs. (18) and (19) and yields a value of $A=4.2\times10^{-14}$ cm^3/sec. The dashed curve of Fig. 3 shows the contributions of the diffusion and three-body terms while the difference between the dashed curve and the solid curve represents the net contribution of the excitation process. At sufficiently low temperatures the $aA(1-R/aM)$ term of Eq. (17) is negligible and the value of γ_M can be found without a knowledge of R/M. Thus, the data of

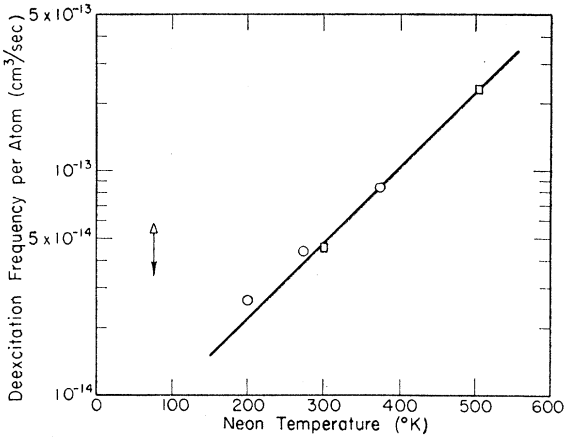

FIG. 8. De-excitation frequencies, A, for the $^3P_1$ to $^3P_2$ transition as a function of neon temperature. The symbols used and sources of data are: (□) from the present work, (○) by Grant and Krumbein, and (△) by Phelps and Molnar.

Phelps and Molnar[6] and of Grant and Krumbein[5] both yield $\gamma_M=5\times10^{-35}$ cc^2/sec at 77°K. Errors in the relative absorption coefficients used in the preceding analyses should cause negligible error in D_M and A as determined from the low neon density data but could cause proportionate errors in the values of A and γ_M determined from the data at high neon densities.

$^3P_1$ Analysis

We are now in a position to analyze the $^3P_1$ equation, Eq. (12). First we note from our analyses of the $^3P_0$ and $^3P_2$ equations that $A/eE\geq80$. From the data of Fig. 4 we conclude that $A(aM/R-1)/eE(S/eR-1)\geq20$ for neon densities less than 5×10^{18} atom/cc. This

[30] The data from reference 5 at 201°K are somewhat suspect since the values of ν_{IR} and γ_M obtained from the same data appear to be low by about a factor of two.

[31] J. R. Dixon, thesis, University of Maryland, 1955 (unpublished). The data are those used to obtain the "theoretical curve" of Fig. 14 of reference 7. The use of the relative absorption coefficients from Table III makes unnecessary the modification of the R/M values used by Dixon to obtain the agreement between theory and experiment.

means that the $eEN(S/eR-1)$ term of Eq. (12) can be neglected to the accuracy of the present calculations. Again, we assume that because of the larger energy discrepancy between initial and final states, $F<A$ so that $fF<1.04\times10^{-3}A$. Therefore, the $fFN(1-T/fr)$ term can be neglected.[28,29] With these assumptions Eq. (12) becomes

$$\nu_{IR}=\nu_R+AN(aM/R-1), \qquad (20)$$

where ν_{IR} is the unknown quantity and $\nu_R=\nu_M$ is the final decay frequency plotted in Fig. 3. The solid circles and squares of Fig. 10 show the ν_{IR} values obtained using Eq. (20) and the data of Figs. 3 and 4. For neon densities greater than 2×10^{17} atom/cc the values of ν_{IR} are independent of neon density and of gas temperature within the accuracy of the data as predicted by

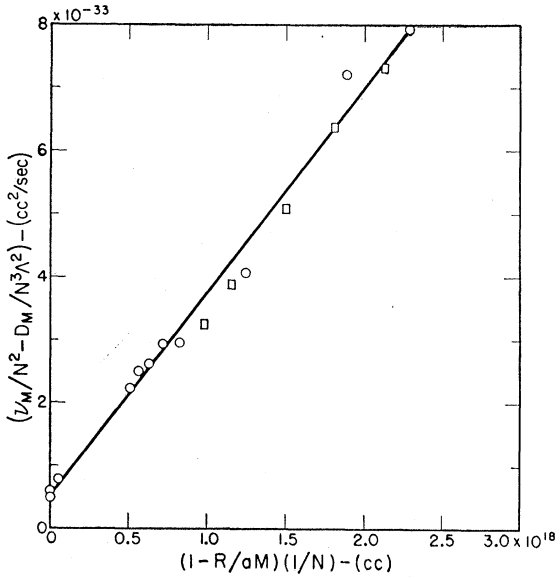

FIG. 9. Determination of two-body and three-body coefficients for the $^3P_2$ state at 300°K using Eq. (19) of the text. The symbols and sources of data are: (○) from the present work with $\Lambda^2=0.050$ cm² and (□) from Dixon with $\Lambda^2=2.48$ cm².

Eq. (10). The average value of ν_{IR} is 5.3×10^4 sec^{-1} as compared to a value of 4.7×10^4 sec^{-1} found using Eq. (10). The tendency of the ν_{IR} values at the lower neon densities to fall below the values at higher neon densities may be due to systematic errors resulting from the difficulties of measurements. However, theory[18] suggests that the ν_{IR} value should pass through a minimum to this region. The absence of a rise in ν_{IR} with gas density at high densities indicates that processes such as collision-induced radiation are negligible. According to Eq. (20) errors in the relative absorption coefficient for the $^3P_2$ and $^3P_0$ states will cause proportionate errors in ν_{IR} when the second term dominates, i.e., at intermediate and low neon densities.

At this point we note that our assumptions leading to Eqs. (17)–(20) are equivalent to assuming that the

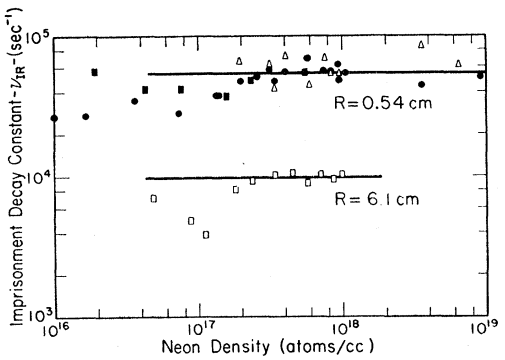

FIG. 10. Imprisonment constant for the $^3P_1$ state and 743A radiation as a function of gas density for different temperatures and different size discharge tubes. The solid circles (●) and squares (■) were calculated using Eq. (20) and data obtained with the $\Lambda^2=0.050$ cm² discharge tube at 300°K and 500°K, respectively. The triangles (△) and squares (□) were calculated using Eq. (21) and data obtained with the $\Lambda^2=0.050$ cm² tube and with a spherical discharge tube with $R=6.1$ cm. The solid lines are drawn through an average of the data for high neon densities.

final decay frequency for the $^3P_2$ and $^3P_1$ states is independent of the properties of the $^3P_0$ and $^1P_1$ states and that the only important two-body collisions are those which cause transition between the $^3P_2$ and $^3P_1$ states. We can now eliminate the R/M ratio from Eqs. (19) and (20) and solve for ν_{IR} to obtain

$$\nu_{IR}=\nu_f+AN\left[\frac{aAN}{\nu_f-D_M/N\Lambda^2-\gamma_M N^2}\right]^{-1}, \qquad (21)$$

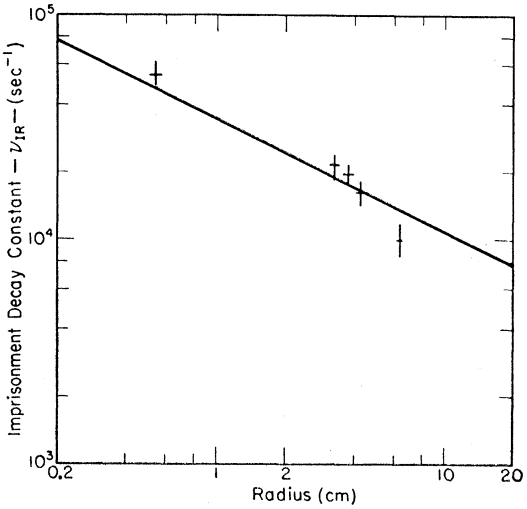

FIG. 11. Variation with imprisonment decay constant for the $^3P_1$ state or 743 A radiation with radius of the discharge tube. The solid line is the prediction of theory as given by Eq. (10). The points at $R=0.54$ cm and 4.3 cm are average of the data for the higher neon densities of Fig. 10. The points at $R=6.4$ cm and 3.3 cm were obtained from the data of Phelps and Molnar while the point at 3.8 cm is from the data of Dixon and Grant. In calculating the imprisonment constant for the sphere of Fig. 10 using Eq. (10) we used an equivalent cylinder radius of $1/\sqrt{2}$ times the actual value. This factor is the same as that which would be needed to convert from cylindrical geometry to parallel plane geometry.

where ν_f is the final decay constant for the $^3P_2$ and $^3P_1$ states. Knowing D_M, A, and γ_M from data such as shown in Figs. 8 and 9 we can use Eq. (21) to find ν_{IR} from experiments in which only ν_f was measured. The open triangles and squares of Fig. 10 show ν_{IR} data obtained using Eq. (21) to analyze the data of Fig. 3 and data obtained by the author for a spherical absorption cell. Figure 11 shows the average ν_{IR} values obtained by applying Eq. (21) to decay frequency data obtained by various workers.[32] The solid line of Fig. 11 shows the predictions of Holstein's theory as given by Eq. (10).

$^3P_0$ Analysis at Late Times

Our analyses of the decay constant and relative density data for the $^3P_2$ and $^3P_1$ levels of neon have neglected the effects of electrons left over from the discharge. The justification for this procedure is that under the experimental conditions used the decay frequency and relative density data used in the analyses were found to be independent of the discharge intensity. However, since previous work[6,7] has shown the $^3P_0$ state to be particularly sensitive to the effects of the electrons, it is necessary to find data which has been taken at low enough discharge intensities to insure that Eq. (13) is applicable. Unfortunately, in our experiments the early decay of the $^3P_0$ density was recorded in only four runs, e.g., Fig. 2. The decay frequencies obtained at early times in these cases are in reasonable agreement with those obtained by Dixon and Grant with very low intensity discharges (see Fig. 5). However, it is important to note that these are the four runs[33] for which we could set only an upper limit to the S/M ratio of Fig. 4. These objections would seem to rule out the use of the final S/M values of Fig. 4, at least for low neon densities. However, we can analyze the initial behavior of time varying relative density data such as shown in Fig. 2 using either Eq. (11) or Eq. (13). Thus, the initial lower value of the $^3P_2$ decay frequency relative to its final value is explained as due to $^3P_2$ production by de-excitation of $^3P_0$ atoms when the $^3P_0$ concentration is relatively large. According to Fig. 2 the changes in ν_M, R/M, and S/M as t changes from 0.5 to 2 milliseconds are $\Delta\nu_M=270$ sec^{-1}, $\Delta R/M=0.0056$, and $\Delta S/M=0.99$. Substitution of these numbers and the value of A from our earlier analyses into Eq. (11) gives $B=6\times10^{-15}$ cm^3/sec. This result suggests that the $^3P_0$ to $^3P_2$ conversion makes up a large fraction of the two-body collisional destruction of the $^3P_0$ state. The difficulties with this analysis are that the changes are small and that the important data is obtained from regions of high absorption where the corrections for nonlinear absorption and a finite photomultiplier gate width are important.[23]

A better method for separating the two-body coefficients for the $^3P_0$ state is to analyze the approach of the S/M ratio to its final value using the data of Fig. 2 and Eq. (13) for a fixed neon density. If we neglect the $gGN(1-T/gS)$ terms for the reasons discussed previously, Eq. (13) can be rewritten in the form

$$\frac{(\nu_S-D_S/N\Lambda^2-\gamma_S N^2)}{(1-eR/S)N}=B\frac{(1-bM/S)}{(1-eR/S)}+E. \quad (22)$$

Here, B and E are the unknowns; ν_S, R/S, and M/S are obtained from data such as shown in Fig. 2; and D_S is the value obtained from Eq. (16). The value of γ_S is unknown, but the term $\gamma_S N^2$ is negligible at the neon densities of these considerations unless it is considerably larger than for the $^3P_2$ metastable. Plots of $(\nu_S-D_S/N\Lambda^2-\gamma_S N^2)(1-eR/S)^{-1}N^{-1}$ as a function of $(1-bM/S)(1-eR/S)^{-1}$ for $N=4\times10^{17}$ and 3×10^{17} atom/cc are shown in Fig. 12 and yield $B=5\times10^{-15}$ cm^3/sec and $E=5\times10^{-15}$ cm^3/sec. The value of $B+E=10\times10^{-15}$ cm^3/sec is in satisfactory agreement with the value of 8×10^{-15} cm^3/sec obtained from Fig. 5. The large scatter in the data at large values of the abcissa corresponds to data obtained early in the afterglow and shows that the data used in the analysis of the preceding paragraph is probably not too reliable.[34]

We now wish to consider whether we can make use of the S/M data at the higher neon densities of Fig. 4 to evaluate the $^3P_0$ three-body collision coefficient, γ_S. In order to estimate the reliability of the S/M data we use Eq. (13) to calculate the final value of S/M from the final value of $\nu_S=\nu_M$ as given in Fig. 3, the value of R/M from Fig. 4, and the values of D_S, B, and E determined above. The calculations must be made at low enough neon densities such that the $\gamma_S N^2$ term can be neglected. The final values of S/M determined in this manner are only 10 and 12% below the upper limits shown in Fig. 4 for 4×10^{17} and 3×10^{17} atoms/cc, respectively. This final value of S/M for a neon density of 4×10^{17} atom/cc leads to the dashed curve of Fig. 2 for the final decay of the $^3P_0$ density. Although the measurements of S/M at neon densities

[32] The variation in ν_{IR} with tube radius provides an explanation for the apparent variation in $^3P_2$ lifetime with the spectral line used for the measurement found by Phelps and Molnar (reference 6). Thus, the 6143 A and 6402 A lines were used to measure the $^3P_2$ decay in absorption cells of 3.3 cm and 6.4 cm radius, respectively.

[33] In these runs a low-voltage low-current pulse lasting for about one millisecond was added to the short high voltage pulse used to break down the gas. Our experience with helium (reference 13) suggests this results in a reduction of the electron density during the afterglow.

[34] The analysis of Eq. (22) and Fig. 12 does not provide unambiguous evidence as to the value of B. For example, if we assume that the 20% change in ν_M in Fig. 2 could be a 10% change, then $B\sim0$ and one would have to introduce into Eqs. (13) and (22) an additional loss process such as collision-induced radiation [reference 13 and E. H. S. Burhop and R. Marriott, Proc. Phys. Soc. (London) **A69**, 271 (1956)] in order to explain the observed $^3P_0$ destruction. However, an analysis similar to that of Eq. (22) and Fig. 12 assuming $B=0$ yields a negative coefficient for the collision-induced radiation frequency and $E=3\times10^{-14}$ cm^3/sec. The latter is much larger than the value of $E+B$ found using Eq. (15) and Fig. 5. We therefore conclude that $B>0$ and that collision induced radiation is probably not an important process.

above 5×10^{17} atom/cc probably were not taken at as low discharge intensities as were the runs at 3 and 4×10^{17} atom/cc, we assume that the increase in the importance of the two-body process will reduce the error due to collisions with electrons and make the values of γ_S obtained by solving Eq. (13) significant. We find a value of $\gamma_S=7\times10^{-35}$ cm^6/sec from the data at 9.2×10^{18} atom/cc. However, the value of $\gamma_S N^2$ is only ten percent of the $\nu_S=\nu_M$ value at this density and becomes negative at lower neon densities. This effect presumably results from values of S/M which are too near the equilibrium value because of excitation from the $^3P_2$ state by electrons. Elimination of ν_M and ν_S between Eqs. (11) and (13) shows that regardless of whether the two-body collisions involve electrons or neutral atoms a value of S/M greater than the equilibrium value implies that the three-body destruction of $^3P_0$ atoms is slower than that for the $^3P_2$ atoms. Errors in the relative absorption coefficients should cause proportionate errors in the ratio of B to E and would cause large errors in γ_S.

VII. DIFFUSION AND DE-EXCITATION COEFFICIENTS FOR EXCITED NEON ATOMS IN HELIUM

Dixon and Grant[7] measured the decay frequencies for neon $^3P_2$ and $^3P_0$ metastables in a mixture of helium and neon. In this section we shall indicate how their results can be analyzed to give the diffusion coefficient and excitation frequencies per atom for neon metastables in pure helium. If we assume that no new processes are introduced by the helium the validity of Eqs. (1) through (22) is unchanged, provided we regard the coefficients as characteristic of the mixture. The

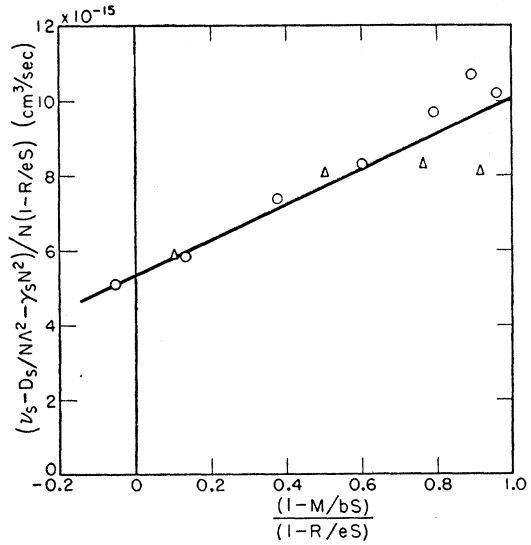

FIG. 12. Determination of the two-body de-excitation frequencies for the $^3P_0-{}^3P_1$ and $^3P_0-{}^3P_2$ transitions using Eq. (22) of the text. The data were obtained at 300°K with $\Lambda^2=0.050$ cm^2. The points shown by circles (○) and triangles (△) are calculated from measurements at neon densities of 4×10^{17} atom/cc and 3×10^{17} atom/cc, respectively.

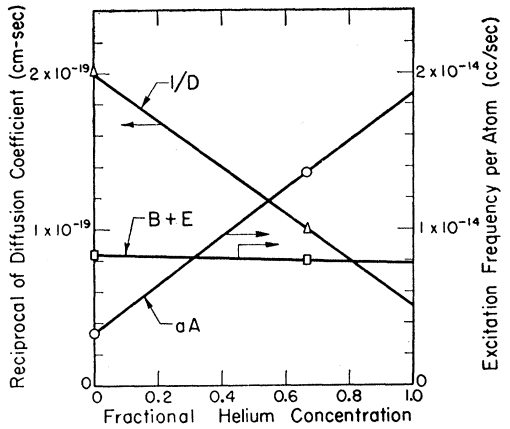

FIG. 13. Determination of the diffusion coefficient, excitation frequencies, and de-excitation frequencies for excited neon atoms at 300°K in helium using Eqs. (23) and (24) to analyze data obtained by Dixon and Grant.

diffusion and two-body coefficients are determined from plots such as Figs. 5 and 6. The diffusion coefficients are related by the equation[35]

$$\frac{1}{D_{yz}}=\frac{x}{D_y}+\frac{1-x}{D_z}=\left(\frac{1}{D_y}-\frac{1}{D_z}\right)x+\frac{1}{D_z}, \qquad (23)$$

where D_{yz}, D_y, D_z are the diffusion coefficients at unit density for an excited atom in the mixture, in gas y, and in gas z, respectively. Here x is the fractional density of gas y in the mixture. Figure 13 shows the available values of the reciprocal of the diffusion coefficients as a function of the fractional concentration of helium. The resultant diffusion coefficient for neon $^3P_2$ and $^3P_0$ metastables in helium is 2×10^{19} cm^{-1} sec^{-1} compared to 5×10^{18} cm^{-1} sec^{-1} for these metastable atoms in neon.

The analysis of the two-body coefficients is based upon a linear superposition of the processes. Thus

$$X_{yz}=\frac{X_yN_y+X_zN_z}{N_y+N_z}=(X_y-X_z)x+X_z, \qquad (24)$$

where X_{yz}, X_y, and X_z are the collision frequencies per atom for metastables in the mixture, in gas y of density N_y and in gas z of density N_z. Figure 13 shows the results of such an analysis using excitation coefficients obtained from Dixon and Grant. The excitation frequency for the $^3P_2$ to $^3P_1$ transition by helium is 1.9×10^{-14} cc/sec. The sum of the de-excitation frequencies for the $^3P_0$ state by helium is 8×10^{-15} cc/sec, as given by Dixon and Grant.

[35] T. Holstein, Phys. Rev. **100**, 1230 A (1955). This work shows that an equation corresponding to Eq. (23) is very accurate for the low-field mobilities of positive ions, μ, provided that the elastic scattering cross section varies in a reasonable manner with ion energy. Equation (23) holds for ions since $D=KT\mu/e$, where e is the electronic charge. Since there is no basic difference between the elastic scattering of ions and of metastables one can use Eq. (23) to relate the diffusion coefficients for metastable atoms.

VIII. ESTIMATES OF ELECTRON-EXCITED ATOM INTERACTIONS

In this section we shall use the observed current dependence of the decay of density of $^3P_2$, $^3P_1$, and $^3P_0$ atoms at high discharge currents to estimate the frequencies of transitions between the excited states of neon caused by thermal electrons. In principle, this requires that simultaneous measurements be made of the electron density[36] and of the decay frequencies and relative densities of the various excited states. However, we can obtain estimates of the electronic excitation and de-excitation frequencies without measuring the electron density if we assume that the electrons are being lost from the afterglow by electron-positive ion recombination. Microwave studies of neon afterglows[37] show that so long as diffusion effects are small, the electron density consistently disappears according to the recombination relation,

$$1/n=1/n_0+\alpha t, \tag{25}$$

where n is the electron density and α is the recombination coefficient of about 2×10^{-7} cm^3/sec at 300°K. The effects of electrons on the decay of the excited atom density can be included in the analysis by adding terms of the form $aA_en(1-R/aM)$, $bB_en(1-S/bM)$, etc., to Eqs. (11)–(13). Here A_e, B_e, etc. are the frequencies of de-excitation per electron and apply to the same initial and final state as do the corresponding coefficients of Table I. For convenience we define a partial decay frequency, β_M, as the difference between the measured value of ν_M and the value of the right hand side of Eq. (11) calculated from the measured relative densities and previously determined coefficients. The equation governing the $^3P_2$ decay can now be written as

$$\frac{1}{n}=\frac{aA_e}{\beta_M}\left(1-\frac{R}{aM}\right)+\frac{bB_e}{\beta_M}\left(1-\frac{S}{bM}\right). \tag{26}$$

As before, we have assumed that processes involving the $^1P_1$ state can be neglected.

If one eliminates n from Eqs. (25) and (26) and evaluates the resulting expression at two values of t separated by Δt one obtains the relation

$$\frac{\Delta t}{\Delta[(1-R/aM)/\beta_M]}=\frac{aA_e}{\alpha}+\frac{bB_e}{\alpha}\frac{\Delta[(1-S/bM)/\beta_M]}{\Delta[(1-R/aM)/\beta_M]}. \tag{27}$$

Here $\Delta(1-R/aM)/\beta_M$ is the difference between values of $(1-R/aM)/\beta_M$ at the times separated by Δt. Similarly for $\Delta[(1-S/bM)/\beta_M]$. Using Eq. (27) and the data given by Dixon and Grant[38] for a 30 milliampere pulsed discharge one can evaluate A_e and B_e. A similar procedure can be used to evaluate A_e and E_e from the $^3P_1$ data and B_e and E_e from the $^3P_0$ data. Unfortunately, the taking of differences to obtain the β's and Δ's results in a large scatter in the data. The data of Dixon and Grant[7] for a 30 ma discharge and by the author for a 20 ma discharge at 6×10^{17} atom/cc and $\Lambda^2=0.05$ cm^2 appear to be consistent with $A_e\approx7.5\alpha=1.5\times10^{-6}$ cm^3/sec, $E_e=\alpha=2\times10^{-7}$ cm^3/sec, and $B_e=\leq\alpha=2\times10^{-7}$ cm^3/sec.

Since $A_e\approx7.5E_e$, we conclude that for the $^3P_1$ data shown by Dixon and Grant at 30 ma the term $eE_en\times(1-S/eR)$ can be neglected compared to the term $A_en(1-aM/R)$. Thus, the drastic change in the $^3P_1$ behavior as the discharge current is increased is due to the excitation of atoms from the $^3P_2$ state to the $^3P_1$ state. Under these conditions the equation for the $^3P_1$ state can be written as

$$\frac{1}{nA_e}=\frac{1-aM/R}{\beta_R}=\frac{1}{n_0A_e}+\frac{\alpha}{A_e}t. \tag{28}$$

Figure 14 shows a plot of $(1-aM/R)/\beta_R$ as a function of time using the data of Dixon and Grant for a 30 ma discharge. From this plot we find $A_e=9\alpha=1.8\times10^{-6}$

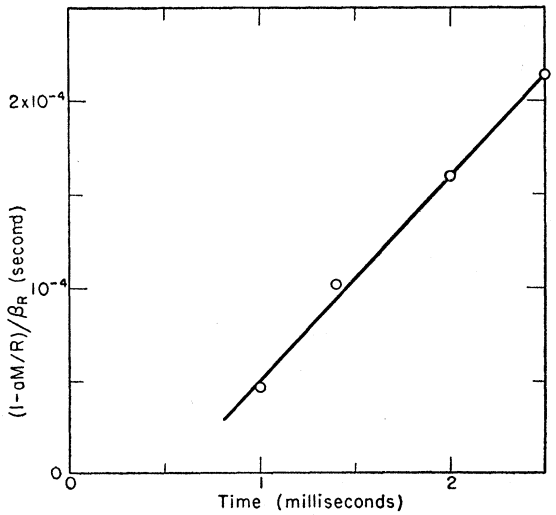

FIG. 14. Determination of de-excitation frequency per electron for the $^3P_1$ to $^3P_0$ transition at 300°K using Eq. (28) of the text.

[36] Blevis, Anderson, and McKay, Can. J. Phys. **35**, 941 (1957). This paper gives the results of simultaneous measurements of the electron density and the absorption by atoms in the $^3P_2$ state.

[37] M. A. Biondi, Phys. Rev. **76**, 1697 (1949); and **93**, 1136 (1954); and H. J. Oskam, Phillips Research Repts. **13**, 335 (1958). The results of these authors show that the loss of electrons by ambipolar diffusion should be negligible under the conditions of the experiments considered here.

[38] Reference 7, Figs. 10, 11, and 13. A reason for departure from Eq. (25) is the production of electrons and positive ions as a result of collisions between pairs of metastables. See M. A. Biondi, Phys. Rev. **88**, 660 (1952). Another reason for departure from Eq. (25) at early times is that the time required for the electrons to reach thermal equilibrium is appreciable. For the conditions of Dixon and Grant's experiment the final decay constant of the excess electron energy is about 500 microseconds. The calculated maximum possible temperature rise of the gas during the 30 milliampere pulse is 5°C.

cc/sec. The apparent negative value of n_0 can be explained by assuming that there is a production of electrons at times less than 0.6 milliseconds.[37,38] Data obtained by the author gives $A_e=6\alpha$ for conditions similar to those of Fig. 2 except that the neon density was 6×10^{17} atom/cc and the discharge current was 20 ma for about 20 microseconds. Note that the frequency of $^3P_2$ excitation, aA_en, is half the frequency of $^3P_0$ de-excitation, E_en, so that the weak current dependence of the $^3P_2$ decay relative to the $^3P_0$ decay is only partially explained by the smaller frequency of $^3P_2$ excitation. One must also take into account the fact that the $^3P_1$ atoms are returned to the $^3P_2$ state with much greater ease ($A_e\sim120eE_e$) than to the $^3P_0$ state so that the net $^3P_2$ destruction is reduced by the presence of significant numbers of atoms in the $^3P_1$ state.

IX. DISCUSSION

The analyses of experimental data in the preceding sections have shown that atoms in the $^3P_2$ metastable state of neon are destroyed upon diffusion to the wall of their container, by collisional excitation to the $^3P_1$ radiating state and by three-body collisions involving two ground state atoms. The atoms in the $^3P_1$ state are destroyed by collisional de-excitation to the $^3P_2$ state and by escape of the imprisoned resonance radiation. Atoms in the $^3P_0$ state are destroyed upon diffusion to the wall and by collisional de-excitation to the $^3P_1$ and $^3P_2$ states and late in the afterglow are produced by collisional excitation from the $^3P_1$ and $^3P_2$ states. Our results show that the final decay frequency, ν_f, for the $^3P_2$, $^3P_1$, and $^3P_0$ states is determined by destruction processes for the $^3P_2$ and $^3P_1$ states and is essentially independent of the collision process involving the $^3P_0$ state. This is expressed in equation form[39] by rewriting Eq. (21) as

$$\nu_f=D/N\Lambda^2+\gamma_MN^2+aAN[1+AN/(\nu_{IR}-\nu_f)]^{-1}. \quad (29)$$

Note that although the last term of this equation is directly proportional to N at low N, ν_f approaches $a\nu_{IR}/(1+a)$ for $AN\ll\nu_{IR}\ll\gamma_MN^2/a$, i.e., large A and small γ_M/a. It is this saturation effect in the net rate of excited atom destruction which led to the nonintegral powers of density or pressure appearing in the earlier attempts to fit theory to the experimental data.[5] The reduction in the limiting contribution of excitation to the $^3P_2$ destruction from ν_{IR} to $a\nu_{IR}/(1+a)$ as a result of de-exciting collisions is probably the most striking feature brought out by this analysis.

Our experiments showed no measurable $^1P_1$ atom density during the afterglow and our analysis is consistent with our assumption that the $^1P_1$ state plays no role in the final decay of the $^3P_{2,1,0}$ density. Early in the afterglow the $^3P_0$ density is relatively large and one observes some production of $^3P_2$ atoms by collisional de-excitation.

[39] Equation (29) reduces to Eq. (23) of reference 2 when $\nu_f\ll\nu_{IR}$.

TABLE IV. Measured de-excitation frequencies per atom and cross sections at 300°K.

Transition	Energy discrepancy (e.v.)	De-excitation frequency (cm³/sec)	Average cross section (cm²)
$^3P_1-{}^3P_2$	0.0517	4.2×10^{-14}	5.2×10^{-19}
$^3P_0-{}^3P_1$	0.0446	5×10^{-15}	6×10^{-20}
$^3P_0-{}^3P_2$	0.0963	5×10^{-15}	6×10^{-20}

The measured diffusion coefficient for the $^3P_2$ state shown in Fig. 7 is proportional to $T^{0.73}$ over the range from 77°K to 500°K. This variation is approximately the same as that observed[13] and calculated[40] for helium metastables and corresponds to an elastic scattering cross section which varies as $v^{-0.46}$, where v is the relative velocity of the colliding particles. The reason for the apparent leveling off of the diffusion coefficient at high temperatures is unknown. The diffusion coefficients for the $^3P_2$ and the $^3P_0$ states are equal to within the experimental error.[7] The mixture experiments show that the diffusion coefficient for neon metastables in helium is about four times that for neon metastables in neon. Since only about a factor of $(3)^{\frac{1}{2}}$ can be accounted for by an increase in the relative velocity of collisions, we conclude that the average cross section for elastic scattering of neon metastables by neon is about twice that for elastic scattering of neon metastables by helium.

The two-body collisional de-excitation frequency per atom for the $^3P_1$ state as shown in Fig. 8 varies by an order of magnitude as the temperature varies from 200°K to 500°K. The strong variation of A with temperature and the relatively small value of all of the de-excitation frequencies are expected in view of the fact that the value of the parameter $\Delta Ed/h\nu$ of the theory of excitation transfer[29] is large, i.e., from 5 to 20 if we take ΔE equal to the spectroscopic separation of the levels, $d=10^{-8}$ cm, and v equal to the mean thermal velocity of the atoms. However, it must be kept in mind that unless we know the details of the interactions between the excited states and the ground state, e.g., the potential energy curves as a function of distance, there is very little we can say about the magnitude of the theoretical expected collision frequencies. The measured de-excitation frequencies and the corresponding average cross sections at 300°K are given in Table IV. Also listed are the energies which are transformed from potential energy into kinetic energy during the excitation transfer process. Although none of our specific assumptions are violated, we see that our general assumption that the de-excitation coefficient decreases with increasing energy discrepancy does not hold for the $^3P_1-{}^3P_2$ transition which has an intermediate energy discrepancy but a very large cross section relative to the others. Since we do not know the details of the interactions, we cannot say whether this is reasonable or not. The mixture experiments show that

[40] R. A. Buckingham and A. Dalgarno, Proc. Roy. Soc. (London) **A213**, 327, 506 (1952).

the frequency of the $^3P_1-{}^3P_2$ de-excitation by helium is six times that produced by neon whereas the frequency of the $^3P_0$ de-excitation is the same for neon and helium. Again, theory is of little help in understanding these observations since we know nothing about the interaction of helium and excited neon atoms. One possible reason for an increase in the de-excitation frequencies with helium is the decrease in $\Delta Ed/\pi v$ due to the increased relative velocity of the colliding particles.

The agreement between our results and the predictions of Holstein's theory of imprisoned resonance radiation is surprisingly good in view of the necessity for estimating the $^3P_1$ radiative lifetime using theory and an uncertain experimental value for the $^1P_1$ radiative lifetime. This appears to be the first experimental check of the imprisonment theory in the region of gas densities in which the rate of escape of radiation is determined by the collisional broadened portion of the spectral line.

The three-body collision coefficients found for the $^2P_2$ state were 5.0×10^{-34} cm^6/sec at 300°K and 5×10^{-35} cm^6/sec at 77°K. These values are larger than those found for helium 2^3S metastables[13] and vary less rapidly with temperature. These observations suggest that if there is a potential maximum in the potential energy *vs* internuclear separation curve for the $^3P_2$ state of neon and a neon atom such as is indicated for the helium 2^3S state,[13,40] the height of the maximum is less than that for helium.

The destruction of atoms in the $^3P_0$ and $^3P_1$ states in collisions with slow electrons has been shown to be a highly probably process. The rough estimates give frequencies of de-excitation per electron of about 10^{-6} cm^3/sec and 10^{-7} cm^3/sec for the $^3P_1$ to $^3P_2$ and $^3P_0$ to $^3P_1$ transitions as compared to a value 3×10^{-7} cm^3/sec for the de-excitation of helium 2^1S_0 metastables to the 2^3S_1 state.[13] In spite of the large value of A_e the decay of atoms in the $^3P_2$ state is relatively unaffected by collisions with electrons because the net rate of $^3P_2$ destruction is reduced by de-excitation of $^3P_1$ atoms. The measured value of A_e corresponds to an average cross section of about 10^{-13} cm^2 or about three times the theoretical limit for electrons with zero angular momentum.[13,41] This apparent violation of the theoretical limit should not be considered too significant in view of the uncertainties of the analysis and scatter in the data used to obtain the electron de-excitation frequencies.

From the preceding discussions one can see the desirability of further experiments to determine (a) the temperature variation of the different two- and three-body collision coefficients, (b) the type of high pressure destruction processes which applies to the $^3P_0$ state, (c) the magnitude and temperature dependence of the electron-excited atom collision coefficients, (d) the effect of pressure on the effective absorption coefficients and, if possible, (e) the collision coefficients for transitions involving the $^1P_1$ state. At present, there are essentially no theoretical results for comparison with the measured diffusion and two-body coefficients so that there is an obvious need for theoretical studies of the interactions of the excited neon atoms with normal neon atoms.

[41] Reference 29, Chap. III. See also E. Baranger and E. Gerjuoy, Phys. Rev. **106**, 1182 (1957).

X. ACKNOWLEDGMENTS

The author wishes to express his appreciation to his associates in the Atomic Physics Group for valuable discussions of this problem. He is particularly indebted to T. Holstein for helpful discussions, and to J. P. Molnar of the Bell Telephone Laboratories for his guidance and interest during the early part of this work.

APPENDIX

Ladenberg[20] and Shortley[10] analyzed the then available data for the dispersion produced by excited neon atoms[20] and for the relative intensities[42] of radiation emitted in transitions from the $2p^53p$ configuration to the $2p^53s$ configuration. Since there appear to be significant errors in this experimental data, the data of Krebs[21] and Garbuny[22] are compared with the predictions of Shortley's theory and are used to obtain a set of relative absorption coefficients. According to Shortley, if one converts the values of relative absorption coefficient and intensity into a set of normalized line strengths arranged as in Tables V and VII the sums of rows and columns should add up to the theoretical values shown.

The results obtained by Krebs[21] give the relative absorption among groups of lines absorbed by atoms in each of the four states of the $2p^53s$ configuration. The measured absorption values were corrected for line reversal effects. Krebs' values for the relative absorption of lines ending on the $^3P_2$ state agree well with the measurements of Dixon and Grant[7] and of the author. Since relative values of line strength are calculated from relative values of the absorption coefficients by dividing by the multiplicity of the lower state, Krebs' results can be tested against Shortley's theory by normalizing the values for a given lower state such that their sum is given by the theoretical sum for the row. This is done in Table V. There is good agreement between the experimental and theoretical values for the sums of columns as shown in the lower two rows.

The measurements of Garbuny[22] give the relative intensities of the lines emitted by atoms in a given state of the $2p^53s$ configuration and are corrected for self-absorption in the source. When these values are multiplied by the cube of the wavelength one obtains the relative line strengths given in Table VI. Here the values have been normalized such that the sum of each column is equal to the theoretical value given in the lowest row. In this

[42] H. G. Dorgelo, Physica **5**, 90 (1925).

TABLE V. Relative line strengths from absorption data.

State J value	p_1 0	p_3 0	p_2 1	p_5 1	p_7 1	p_{10} 1	p_4 2	p_6 2	p_8 2	p_9 3	Theoretical sum
$^3P_2$			5.5	2.1	4.0	18.2	10.5	26.2	16.7	66.9	150
$^3P_1$	V.S.	10.7	3.3	V.S.	19.2	7.4	15.8	4.5	29		90
$^1P_1$	11.8	V.S.	13.5	13.8	V.S.	?	24	20.9	4.0		90
$^3P_0$			9.1	12.2	6.7	2.0					30
Experimental sum	11.8	10.7	31.4	28.1	29.9	27.6	50.3	50.6	49.7	66.9	360
Theoretical sum	10	10	30	30	30	30	50	50	50	70	360

TABLE VI. Relative line strengths from emission data.[a]

State J value	p_1 0	p_3 0	p_2 1	p_5 1	p_7 1	p_{10} 1	p_4 2	p_6 2	p_8 2	p_9 3	Experimental sum	Theoretical sum
$^3P_2$			3.7	1.4	2.9	17.5	6.4	18.2	15.6	70	135.7	150
$^3P_1$	0.1	9.8	2.2	0.3	18.0	7.5	12.2	3.6	27.1		80.8	90
$^1P_1$	9.9	0.2	17.3	16.7	2.4	2.7	31.4	28.2	7.3		116.1	90
$^3P_0$			6.8	11.6	6.7	2.3					27.4	30
Theoretical sum	10	10	30	30	30	30	50	50	50	70	360	360

[a] The p_{10} to $^1P_1$ (8082 A) value is taken as the value necessary to make the sum of the values in the p_{10} column equal to the theoretical value. Also the $p_9 - {}^3P_2$ value is equal to its theoretical value by construction.

TABLE VII. Averaged line strengths from emission and absorption data.

State J value	p_1 0	p_3 0	p_2 1	p_5 1	p_7 1	p_{10} 1	p_4 2	p_6 2	p_8 2	p_9 3	Experimental sum	Theoretical sum
$^3P_2$			4.3	1.6	2.9	14.6	7.4	19.1	12.5	66.3	128.7	150
$^3P_1$	0.1	9.8	2.7	0.3	18.3	6.6	13.8	4.0	23.9		79.5	90
$^1P_1$	13.0	0.2	18.5	17.2	2.4	2.7	32.3	27.5	5.6		119.4	90
$^3P_0$			9.3	13.3	7.7	2.1					32.4	30
Experimental sum	13.1	10.0	34.8	32.4	31.3	26.0	53.5	50.6	42.0	66.3	360.	
Theoretical sum	10	10	30	30	30	30	50	50	50	70		360

case there is rather poor agreement between the experimental and theoretical values for the sums of rows.

Table VII shows a statistical average of the relative line strengths obtained for us by Hook and Jeeves[43] from the two sets of relative experimental values given in Tables V and VI. The results of the averaging are normalized to make the sum of all values equal to 360. The agreement between theory and experiment is even poorer using the averaged results than when using the emission data.

As was observed by Shortley using the earlier data, a striking feature of Tables VI and VII is that the line strengths for transitions ending on the $^1P_1$ state are much larger than predicted by theory. If one accepts the theory as correct, then one would be forced to conclude that the emission measurements are in error and use the relative line strengths of Table V. If one questions the theory, the averaged experimental values of Table VII are the best available. We have made the assumption that the values of Table VII are correct. The relative absorption coefficient for the lines of interest in our analysis are found by dividing the relative line strengths by the multiplicity of the lower state and are listed in Table III. Fortunately, the differences between the relative absorption coefficients obtained from the values of Tables VI and VII for the lines of importance to us are only about 20%.

[43] R. Hook and T. A. Jeeves (private communication).